The impact of organic nitrates on summer ozone formation in Shanghai, China

Chunmeng Li[1], Xiaorui Chen[2, 3 *], Haichao Wang[2, 3], Tianyu Zhai[4], Xuefei Ma[5], Xinping Yang[4], Shiyi Chen[5], Min Zhou[6], Shengrong Lou[6], Xin Li[5], Limin Zeng[5], Keding Lu[5*]

[1] Center for Environmental Metrology, The National Institute of Metrology, Beijing 100029, China.
[2] School of Atmospheric Sciences, Sun Yat-sen University, Zhuhai, Guangdong, 519082, China.
[3] Guangdong Provincial Observation and Research Station for Climate Environment and Air Quality Change in the Pearl River Estuary, Key Laboratory of Tropical Atmosphere-Ocean System, Ministry of Education, Southern Marine Science and Engineering Guangdong Laboratory (Zhuhai), Zhuhai, 519082, China.
[4] State Environmental Protection Key Laboratory of Vehicle Emission Control and Simulation, Chinese Research Academy of Environmental Sciences, Beijing, 100012, China
[5] State Key Joint Laboratory of Environmental Simulation and Pollution Control, The State Environmental Protection Key Laboratory of Atmospheric Ozone Pollution Control, College of Environmental Sciences and Engineering, Peking University, Beijing, 100871, China.
[6] State Environmental Protection Key Laboratory of the Cause and Prevention of Urban Air Pollution Complex, Shanghai Academy of Environmental Sciences, Shanghai, 200233, China.

* Correspondence: chenxr95@mail.sysu.edu.cn; k.lu@pku.edu.cn

Abstract

Organic nitrates serve as important secondary oxidation products in the atmosphere, playing a crucial role in the atmospheric radical cycles and influencing the production of secondary pollutants (ozone (O_3) and secondary organic aerosols). However, field measurements of organic nitrates are scarce in China, and a comprehensive localized mechanism for organic nitrates is absent, hindering effective pollution mitigation strategies. In this study, we conducted measurements of ambient gaseous organic nitrates and examined their effects on local O_3 production at a polluted urban site in eastern China during summer. The average daytime concentrations of alkyl nitrates (ANs) and peroxy nitrates (PNs) throughout the campaign were 0.5±0.3 ppbv and 0.9±0.7 ppbv, respectively, with peaks reaching up to 1.6 ppbv and 3.6 ppbv. An observation-constrained box model, incorporating an updated mechanism for organic nitrates, was employed to assess the environmental impact of these compounds. The model results indicated that PNs production inhibited the daytime O_3 production by 16% (0.8 ppbv/h), which is relatively low compared to previous studies. Furthermore, scenario analyses revealed that production yields (α) of ANs would alter the response of O_3 formation to precursors due to varying compositions of volatile organic compounds. Our results suggest that blind pollution control may cause ineffective pollution prevention and highlight the necessity of a thorough understanding on organic nitrate

chemistry for local O_3 control strategy.

1. Introduction

Tropospheric ozone, as an important oxidant, influences the atmospheric lifetimes of trace gases through its involvement in photochemical processes, thereby playing a crucial role in climate change and atmospheric chemistry. There is a broad consensus that high near-surface ozone concentrations are hazardous to human health and environmental ecosystems, particularly affecting the human respiratory and cardiovascular systems, and result in decreased yields of various crops (Ashmore, 2005; Xue and Zhang, 2023). A scientific assessment of tropospheric ozone is essential for the development of public health policies and for addressing long-term air pollution challenges (Monks et al., 2015). Primary pollutants, such as nitrogen oxides (NO_x) and volatile organic compounds (VOCs), participate in the formation of HO_x radicals ($RO_x = RO_2 + HO_2 + OH$) cycles and NO_x cycles under sunlight, leading to the continuous production of ozone as a secondary oxidation product within these cycles. In addition to the reaction between OH and NO_2 that produces HNO_3 as part of chain termination reactions, the interaction of RO_2 and NO that produces organic nitrates is of increasing concern (Present et al., 2020). The atmospheric production of organic nitrates consumes both NO_x and RO_2. Therefore, the chemistry of organic nitrates will significantly influence the prevention and control of ozone, with NO_x and VOCs serving as independent variables.

Both anthropogenic activities and natural processes contribute to the emissions of NO_x and VOCs, which produce RO_2 in the presence of oxidants such as OH. Subsequently, RO_2 reacts with NO to yield NO_2 and RO. After that, NO_2 photolysis produces O_3, while RO is converted into HO_2 through an isomerization reaction, thereby forming the ozone production cycle. Within the cycle, a branching reaction between RO_2 and NO leads to the formation of alkyl nitrates ($RONO_2$, ANs), while RO_2 may also react with NO_2 to generate peroxy nitrates (RO_2NO_2, PNs). Given that PNs are prone to thermal dissociation near the surface (Roberts and Bertman, 1992), they can influence O_3 production by modifying the availability of NO_x and RO_x. Due to the competitive production dynamics between PNs and O_3, numerous field observations and model simulations have been conducted to investigate the impact of peroxyacetyl nitrate (PAN) on O_3 production (Liu et al., 2021; Zeng et al., 2019; Zhang et al., 2020). For ANs formation, the branching ratio (α), the reaction ratio $k_{1b}/(k_{1a}+k_{1b})$, varies between 0.1-35%, which are associated with the carbon chain structure of the molecule, the distribution of functional groups, temperature, and pressure (Reisen et al., 2005;Arey et al., 2001;Wennberg et al., 2018;Russell and Allen, 2005;Butkovskaya et al., 2012;Cassanelli et al., 2007). Some values of α, which have not been quantified in the laboratory, are estimated through structure-activity relationships (Arey et al., 2001; Reisen et al., 2005; Teng et al., 2015; Yeh and Ziemann, 2014a; Yeh and Ziemann, 2014b). Multiple field observations revealed a strong linear correlation between ANs and O_3, with a correlation coefficient (r^2) exceeding 0.5, further substantiating the competitive relationship between ANs and O_3 (Aruffo et al., 2014; Day et al., 2003; Flocke et al., 1998).

$$RO_2+NO \rightarrow RO+NO_2 \text{ (R1a)}$$

$$RO_2+NO \rightarrow RONO_2+NO_2 \text{ (R1b)}$$

Currently, research on the effects of ANs on O_3 distribution is predominantly located in Europe and the United States. Following the first in situ measurement of total organic nitrates through thermal dissociation laser-induced fluorescence instrument (TD-LIF) by Day et al., field observations of total ANs have been continuously conducted to study the role of ANs in the nitrogen cycle (Aruffo et al., 2014; Browne et al., 2013; Chen et al., 2017; Darer et al., 2011; Day et al., 2003; Sadanaga et al., 2016). In conjunction with field observations and model simulations, Farmer et al. were the first to indicate that ANs influence the sensitivity of NO_x-VOCs-O_3 (Farmer et al., 2011). As NO_x emissions decrease due to pollution control measures, ANs chemistry is expected to play an increasingly significant role in O_3 simulations (Present et al., 2020; Zare et al., 2018). Current mechanisms for O_3 simulations generally achieve reasonable predictions in large-scale models; however, they exhibit deviations exceeding 10 ppbv in regional simulations (Young et al., 2018). Subsequent studies have demonstrated that refining the ANs chemistry can further improve the simulation performance for O_3 (Schwantes et al., 2020). ANs are predominantly produced through oxidation reactions facilitated by OH, O_3, and NO_3. The daytime ANs are mainly contributed by the OH channel, whereas during nighttime, the contribution of the NO_3 channel is linked to significantly increased yields of ANs (Liebmann et al., 2018; Ng et al., 2017; Zare et al., 2018). Presently, the enhancement of ANs chemistry mainly focuses on BVOCs, particularly isoprene and monoterpenes. These researches aim to enhance the yield of ANs derived from BVOCs, the re-release ratio of ANs to $NO_{x,}$ and the contribution of ANs to aerosols (Fisher et al., 2016; Romer et al., 2016; Travis et al., 2016; Zare et al., 2018). Despite the establishment of a complete mechanism scheme at present, significant uncertainties remain in ANs simulation, which may introduce substantial uncertainties into the O_3 simulation.

Atmospheric pollution is common across China, particularly in the Yangtze River Delta. Shanghai, as a highly urbanized metropolis in the Yangtze River Delta, has rendered the region's complex pollution due to its rapid economic growth and urbanization (Wang et al., 2022; Zhu et al., 2021). Previous studies have shown a significant increase in near-surface O_3 levels from 2006 to 2016 in Shanghai (Gao et al., 2017). However, research on the ANs chemistry and their impact on O_3 pollution remains limited in this area. In addition, most field measurements of ANs have focused on short-chain species (Ling et al., 2016; Song et al., 2018; Sun et al., 2018; Wang et al., 2013), which have been observed to exert a typical inhibition effect on daytime O_3 production. A limited number of total ANs measurements found that both ANs and O_3 production were in the VOC-limited regime (Li et al., 2023). To further investigate the influence of organic nitrates on O_3 production, this study describes the distribution of organic nitrates based on a comprehensive field campaign conducted in Shanghai, analyzes the effects of organic nitrates on O_3 production through model simulations, and offers recommendations for the prevention and control of ozone pollution in the region.

2. Methodology

2.1 Measurement site and instrumentations

A comprehensive campaign was conducted in Shanghai to further investigate the chemical behavior of organic nitrates in urban environments across China. As depicted in Fig. 1, the site is located in the Xuhui District of Shanghai (121.44°E, 31.18°N), in proximity to the Shanghai Inner Ring Viaduct, surrounded by numerous residential and office areas without significant industrial emission sources. The site is mainly influenced by morning-evening rush hours, as well as the transport of air masses to the urban location. The overall wind speed was low, predominantly originating from the east. All the measurement instruments were housed in the temperature-controlled room within the laboratory building at the Shanghai Academy of Environmental Sciences. Thermal Dissociation-

Cavity Enhanced Absorption Spectroscopy (TD-CEAS) was positioned on the 7th floor about 25 m above ground level, with the sampling tube extending out through the window.

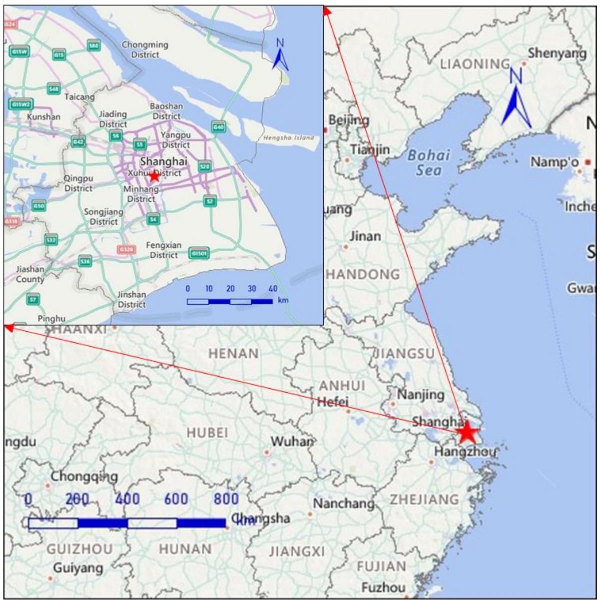

Figure 1. Map of the city of Shanghai and the surrounding area (@ MeteoInfoMap). The red star is the location of the campaign site.

The Shanghai campaign focused on studying summer ozone pollution, with the chemical parameters presented in Table 1. Organic nitrates were measured by TD-CEAS with a sampling flow rate of 3 L/min and a sampling duration of 3 min for alternating measurements of NO_2, PNs, and ANs. The sampling apparatus consisted of a 2-meter-long 1/4-inch tetrafluoroethylene (TFE) tube, through which the atmosphere was filtered through a TFE particulate filter. The membrane was replaced once a day to mitigate the interference caused by wall loss. The measurement of PAN was conducted by gas chromatography electron capture detection (GC-ECD). The Measurement of N_2O_5 was performed via CEAS, which relies on the thermal dissociation of N_2O_5 to yield NO_3. Particulate nitrates and gaseous HNO_3 were measured online by AeRosols and GAses (MARGA), where soluble substances were quantified through ion chromatography following dissolution. The measurements of HONO were finished by CEAS during the campaign. Measurements of VOCs were achieved using a combination of GC-FID and GC-MS, with GC-MS predominating due to the limited species measured by GC-FID. The photolysis rate constant (J value) was determined using a spectrum radiometer with a time resolution of 20 s. Additionally, simultaneous measurements of other trace gases such as NO, NO_2, SO_2, CO, O_3, and $PM_{2.5}$ were conducted using commercial instruments.

Table 1. Measured species for organic nitrates analysis and instrument time resolution, accuracy, and detection limitation.

Parameters	Measurement technique	Time resolution	Accuracy	Detection limit
ANs, PNs, NO_2	TD-CEAS	3 min	± 8%	93 pptv
PAN	GC-ECD	5 min	± 10%	5 pptv
N_2O_5	CEAS	1 min	± 19%	2.7 pptv
NO	Thermo 42i	1 min	± 10%	60 pptv

NO_2	Chemiluminescence	1 min	± 10%	300 pptv
HONO	CEAS	1 min	± 3%	100 pptv
Particulate nitrate	2060 MARGA	1 h	± 3%	0.01 μg/m^3
HNO_3	2060 MARGA	1 h	± 3%	0.01 μg/m^3
SO_2	Thermo 43i-TLE	1 min	± 16%	50 pptv
HCHO	Hantzsch fluorimetry	1 min	± 5%	25 pptv
CO	Thermo 48i-TLE	1 min	± 16%	50 pptv
O_3	Thermo 49i	1 min	± 5%	0.5 ppbv
$PM_{2.5}$	Thermo TEOM	1 min	± 5%	0.1 μg/m^3
VOCs	GC-FID/GC-MS	1 h	± 30%	20-300 pptv
J value	Spectrum radiometer	20 s	± 10%	5×10^{-5} s^{-1}

2.2 Model calculation

To investigate the impact of ANs chemistry on O_3 production, a box model was employed to simulate the photochemistry processes. The mechanism of the model was enhanced based on RACM2 (Regional Atmospheric Chemical Mechanism version 2). This box model simulates the physicochemical processes occurring within a defined volume for each reactant. It utilizes measured parameters as the boundary condition to simulate the chemistry process while allowing for convenient adjustments to the mechanism. The model generates files detailing concentration changes, budget processes, and reaction rates, thereby providing an efficient means to simulate ground-level pollutants. In this study, the box model was constrained by various parameters, including J values, O_3, NO, NO_2, CO, HONO, VOCs, RH, temperature, and pressure, with the time step set to 1h. The deposition process was quantified using the deposition rate and the boundary layer height, with the dry deposition rate established at 1.2 cm/s and the boundary layer height constrained by data obtained from NASA.

The RACM2 facilitates classification through the distribution of functional groups and subsequently delineates reactions involving 17 stable non-organic compounds, 4 inorganic intermediates, 55 stable organic compounds, and 43 intermediate organic species within the mechanism. However, the mechanism description for ANs is notably abbreviated. The various ANs, characterized by differing functional groups, are treated as a unified entity, thereby neglecting the influence of functional groups on the underlying chemistry. Consequently, this study builds on the previous research and further evaluates the updates of the mechanism (Li et al., 2023). These mechanistic updates are developed based on the work of Zare et al. and primarily encompasses the oxidation processes of BVOCs by OH and NO_3, as well as the deposition and the aerosol uptake, which are detailed in the SI (Zare et al., 2018). Accordingly, three mechanistic schemas are compared based on the campaign, which will be elaborated upon in subsequent sections. A box model based on the above mechanism is used to calculate the ozone production rate ($P(O_3)$) (Tan et al., 2017b). $P(O_3)$ was quantified based on the net production rate of O_x (the sum of O_3 and NO_2), by subtracting the O_x depletion from the instantaneous O_x production. The simulation uncertainty of the box model is about 40%, introduced mainly by the simplified reaction rate constants, photolysis rate constants, and near-ground deposition (Lu et al., 2013). The impact of PNs photochemistry on local ozone is quantified by comparing the difference of the daytime $P(O_3)$ between the scenarios with and without PNs photochemistry via a chemical box model. Here, the PNs photochemistry includes the production and removal of PAN, MPAN and PPN.

To facilitate the assessment of the impacts of ANs on local O_3 pollution, we further conducted a simplified box model based on the steady-state assumption approach. Several studies have examined the combined effect of α and VOCs reactivity on local O_3 levels using this approach (Farmer et al., 2011; Present et al., 2020; Romer et al., 2016; Romer et al., 2018). Briefly, the production pathway of ANs is simplified according to VOCs categories and the production rate of OH and HO_2 ($P(HO_x)$) is fixed to a constant value. VOCs are categorized into two primary groups: non-oxygenated VOCs (RVOCs) and oxygenated VOCs (OVOCs). Both categories of VOCs undergo oxidation by OH, resulting in the formation of RO_2, specifically $RVOCRO_2$ and $OVOCRO_2$. The interaction between $RVOCRO_2$ and NO will produce α ANs, (1-α) NO_2, HO_2, and OVOC. Conversely, the reaction of $OVOCRO_2$ with NO directly generates NO_2. In the Beijing-Tianjin-Hebei, Yangtze River Delta, and Chengdu-Chongqing regions of China, $P(HO_x)$ is approximately 4 ppbv/h (Lu et al., 2013; Tan et al., 2018a; Tan et al., 2018b). $P(HO_x)$ is therefore assumed to be 4 ppbv/h, with equal production rates of OH and HO_2. The model also incorporates additional processes, including inter- and self-reactions of RO_2, as well as reactions between NO_2 and NO, and deposition processes. In addition, during the daytime, NO is determined by $j(NO_2)$, O_3, and NO_2 according to the photo-stationary state among NO-NO_2-O_3. Based on the above simplified approach, production rates of ANs and O_3 in this study can be derived by direct calculations.

To investigate the effects of NO_x and VOCs on O_3 production, the theoretical maximum of $P(O_3)$ was simulated by a box model under varying concentrations of NO_x and VOCs. This approach was employed to develop an empirical kinetic modeling approach for ozone production (EKMA). The EKMA serves as a model sensitivity method to inform strategies for pollutant abatement. In this study, EKMA utilizes the measured mean parameters as the initial point. Each parameter was incrementally adjusted in 30 equidistant steps to create scaled arrays of VOCs and NO_x, which were subsequently used to simulate the variations in $P(O_3)$ resulting from changes in precursor concentrations. Ultimately, contour plots illustrating the relationship between $P(O_3)$ arrays versus the concentrations of NO_x and VOCs are plotted based on the simulation results.

3. Results and discussions

3.1 Overview of organic nitrates and precursors

The duration of the Shanghai campaign was 20 days, spanning from May 25 to June 13, 2021. The analysis of organic nitrates is performed from 6 a.m. to 6 p.m., as measurements taken during nighttime were subject to interference from N_2O_5 and its derivatives, a phenomenon noted in previous studies (Li et al., 2021; Li et al., 2023). Simultaneous measurements of PAN and PNs were conducted throughout the campaign. There was a malfunction of the GC-ECD instrument from June 12 to June 13, during which the measurements of PAN were generally low. Relative humidity (RH) varied considerably, with over 95% during rainfall periods on June 2, June 9, June 10, and June 13, while the remaining days were predominantly sunny. Temperatures were high, with minimums of 20 °C and daytime peaks reaching up to 36 °C. The wind speeds were generally high during the daytime and low at night, with maximum of 4.2 m/s. The easterly winds prevailed during the campaign, except for May

27-28 and June 3-6 with mostly west and southwest winds.

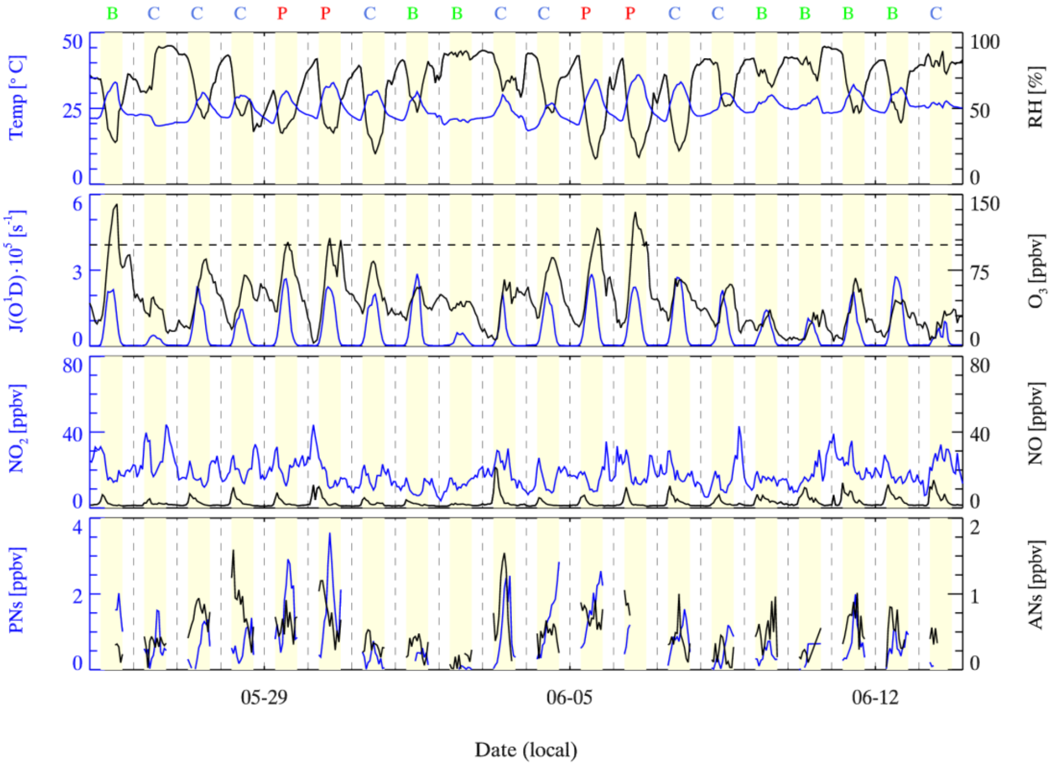

Figure 2. The time series of the related parameters focused on organic nitrates during the campaign. The background days are represented by green B, the clean days are represented by blue C, and the ozone pollution day is represented by red P.

According to Chinese air quality standards for Class II areas, which define ozone pollution days as those with an hourly average exceeding 100 ppbv, the periods from May 29 to May 30 and June 5 to June 6 have been identified as ozone pollution days. The days without ozone pollution are categorized as clean or background days. For clean days, parameters, including K_{OH}, SO_2, and CO, show significant diurnal variations (Fig S1), and no rain occurs. The days that are neither ozone pollution days nor clean days are then classified as background days. The daytime averages of environmental parameters during the ozone pollution period, the clean period, and the background period are presented in Table 2. Excluding cloudy and rainy days, the daytime peak of $J(O^1D)$ was near 2.8×10^5 s^{-1}, indicating a high photochemical oxidation potential. As a secondary photochemical product, O_3 exhibited a typical daily profile, peaking at 140.5 ppbv throughout the campaign. The measurements of PNs peaked at 3.6 ppbv with a daytime average of 0.5 ± 0.3 ppbv, while ANs peaked at 1.6 ppbv with a daytime average of 0.5 ± 0.3 ppbv. Ozone pollution periods were often associated with high organic nitrates. The mean daily variation of NO_x was consistent with the characteristics of typical urban sites, significantly influenced by the morning-evening rush hours. During the daytime, NO exhibited a single peak distribution, whereas NO_2 displayed a bimodal distribution. In comparison to the background and clean period, the ozone pollution period was characterized with higher temperatures and lower humidity. Additionally, the photolysis rate and levels of $PM_{2.5}$ were both elevated during pollution days.

Table 2. Summary of daytime averages of chemical parameters over different periods during the Shanghai campaign.

Pharse	Ozone pollution	Background	Clean
T/°C	29.8±3.7	27.0±3.4	26.0±3.5
P/hPa	1043.6±0.8	1045.3±0.9	1044.3±1.4
RH/%	39.2±13.9	65.2±16.0	62.4±17.2
J(O^{1}D)×10^5/s	1.3±0.9	0.9±0.8	0.8±0.8
J(NO$_2$)×10^3/s	4.5±2.1	2.8±2.0	2.6±1.9
NO$_2$/ppbv	17.3±6.1	16.5±5.8	20.3±7.4
NO/ppbv	3.2±2.6	4.0±2.7	4.2±3.7
O$_3$/ppbv	78.6±30.9	41.6±27.7	45.0±21.5
PM$_{2.5}$/μg·m^{-3}	25.9±4.3	18.3±13.4	21.9±10.0
SO$_2$/ppbv	2.2±1.7	0.4±0.5	0.6±0.7
CO/ppbv	505.3±64.3	441.6±133.3	535.0±147.8
ISO/ppbv	0.1±0.1	0.2±0.2	0.1±0.1

The mean diurnal profiles of organic nitrates and related parameters observed during the campaign are shown in Fig. 3. During the ozone pollution period, NO$_x$ exhibited a peak concentration at 3:00 a.m., indicating the transport of a polluted air mass to the site. In comparison to the clean period, daytime NO$_x$ was lower during the ozone pollution period, particularly at noon when NO dropped to as low as 1.7 ppbv. Correspondingly, ANs during the ozone pollution period were generally high, but the daily variation was not significant. Therefore, the sources of ANs were more complex during the ozone pollution period, involving both transport contribution and local production, which aligns with the significantly increased background O$_3$. During the clean period, the daytime peak of O$_3$ was notably reduced and occurred later in the day. The fluctuations in NO$_x$ were more closely associated with morning and evening rush hours. The daytime peak of PNs decreased from 2.6 ppbv to 1.4 ppbv. In addition, the diurnal profile of ANs displayed a more pronounced peak at noon. During the background period, there was a further decline in the daytime peaks of NO$_x$ compared to the clean period. The diurnal profile of O$_3$ exhibited similar trends, but the duration of high O$_3$ was significantly shortened. The levels of both PNs and ANs exhibited a decline, approaching the background concentrations.

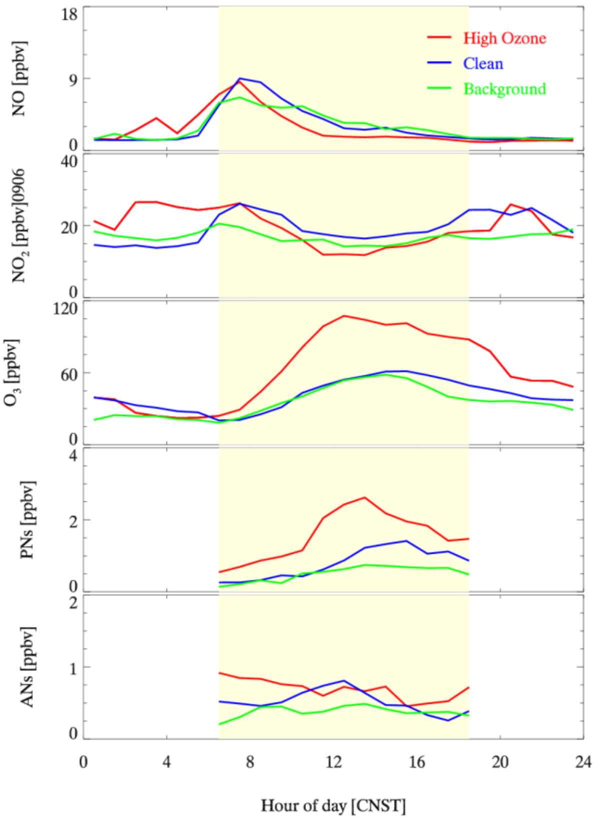

Figure 3. Mean diurnal profiles of organic nitrates and related parameters during different observation periods.

Here, we compare our observations with the study previously conducted in Xinjin, which is a suburban site, located in basin topography and faces emerging ozone pollution recently, to determine the effect of organic nitrate on O_3 production under different pollution conditions (Li et al., 2023). The Shanghai and Xinjin campaigns were conducted in early and late summer, respectively, exhibiting similar meteorological conditions. Photochemical conditions during both two campaigns are comparable, with the daily means of $J(O^1D)$ were 0.9×10^{-5} s^{-1} and 0.8×10^{-5} s^{-1}, while the daily means of $J(NO_2)$ were 3.1×10^{-3} s^{-1} and 3.0×10^{-3} s^{-1}, respectively, during Shanghai and Xinjin campaigns. The ratio of NO to NO_2 was 0.19 and 0.17 at Shanghai and Xinjin, respectively. Meanwhile, the concentration of NO_x observed in Shanghai site (daily averages of 22.0 ppbv) is higher than that observed in Xinjin site (daily averages of 12.5 ppbv). The concentrations of SO_2 and CO at Shanghai site were 0.9 and 491.4 ppbv, while SO_2 and CO were 0.6 and 404.5 ppbv, respectively. Therefore, the air masses at Shanghai site were less aged than Xinjin site. However, the concentration of VOCs is lower in Shanghai campaign compared to Xinjin campaign, with daily mean of 23.5 ppbv compared to 22.4 ppbv. Therefore, a comparison of the two campaigns facilitates a comprehensive analysis of the impacts of organic nitrate chemistry on local ozone pollution.

3.2 Evaluation of organic nitrates simulations

In light of the updates to the mechanisms, validation testing has been conducted. Our previous study of the Xinjin campaign evaluated three mechanism schemes: mechanism S0, which is based on RACM2, mechanism S1 and mechanism S2 which refines the budget for BVOC-derived organic nitrates (Li et al., 2023). It was found that the performance of mechanism S2 for organic nitrates exhibited an improvement exceeding 50%. Mechanism S2 has been updated by the Berkeley group (Fisher et al., 2016; Travis et al., 2016), which includes enhancements to the production mechanism of isoprene, the incorporation of the production mechanism for monoterpenes, and the completion of the uptake of organic nitrates by aerosols. Additionally, the Zare mechanism further refines the production mechanism of organic nitrates initiated by OH and NO_3, as well as improving the deposition process of organic nitrates. As a result, the Shanghai campaign was simulated using RACM2, Berkeley, and Zare mechanisms respectively for comparison.

The simulation result of organic nitrates under the three mechanisms is shown in Fig. 4a. The simulations for PAN or PNs exhibit an overall underestimation tendency, with the simulation of PAN demonstrating an even greater underestimation. Notably, the measured PNs remained above 500 pptv during nighttime, indicating a continuous transportation contribution at this site. Furthermore, the underestimation of PNs may be attributed to the unidentified RO_x sources. It is consistent with the findings from summer campaigns in Wangdu, Beijing, where an underestimation of RO_2 was noted, particularly pronounced at elevated ambient NO_x (Tan et al., 2017a). In terms of ANs, the simulation performances vary across different mechanisms. A significant overestimation of ANs is evident when utilized RACM2. Conversely, the simulation based on the Berkeley and Zare mechanisms generally results in an underestimation of ANs, while the underestimation of the Zare mechanism is more significant. Sensitivity tests conducted in Xinjin campaign suggested that the simple representation of ANs uptake caused the underestimation (Li et al., 2023), which is the same reason of underestimation in the Shanghai campaign. The uptake of ANs need further experimental data to achieve a detailed description to support the simulations.

The diurnal profile of simulated PNs is consistent with the measurements, both reaching their daytime peak shortly after sunrise. However, it is noteworthy that the peak concentration of PNs measurements is significantly higher than the simulation. In a similar pattern with PNs, the simulated ANs began to accumulate around 6:00 a.m. The measured ANs reached their peak near noon, whereas the simulations peaked at 3:00 pm. To evaluate the performance of simulations, as showed in Fig. 4b, three types of error ratios were calculated: Mean Square Error (MSE), Mean Absolute Error (MAE), and Mean Absolute Percentage Error (MAPE). Different error metrics for the organic nitrates exhibit a similar trend. The simulation performances of the Berkeley mechanism are better than the other two mechanisms. It should be noted that the Berkeley mechanism failed to fully reproduce the diurnal pattern of observed ANs. This is mainly due to the atmospheric transport that contributes to the ANs as mentioned in section 3.1. In addition, the drastic changes in NO_x during rush hours will introduce errors to the ANs measurements. In addition, the Zare mechanism refined the oxidation of BVOCs by OH or NO_3 by introducing extra species with uncertain yields, which might bring biases to the simulations under high NO_x and anthropogenic VOCs. In general, the Berkeley mechanism performs better on simulation of ANs than Zare mechanism. As a result, the subsequent analysis is based on the Berkeley mechanism.

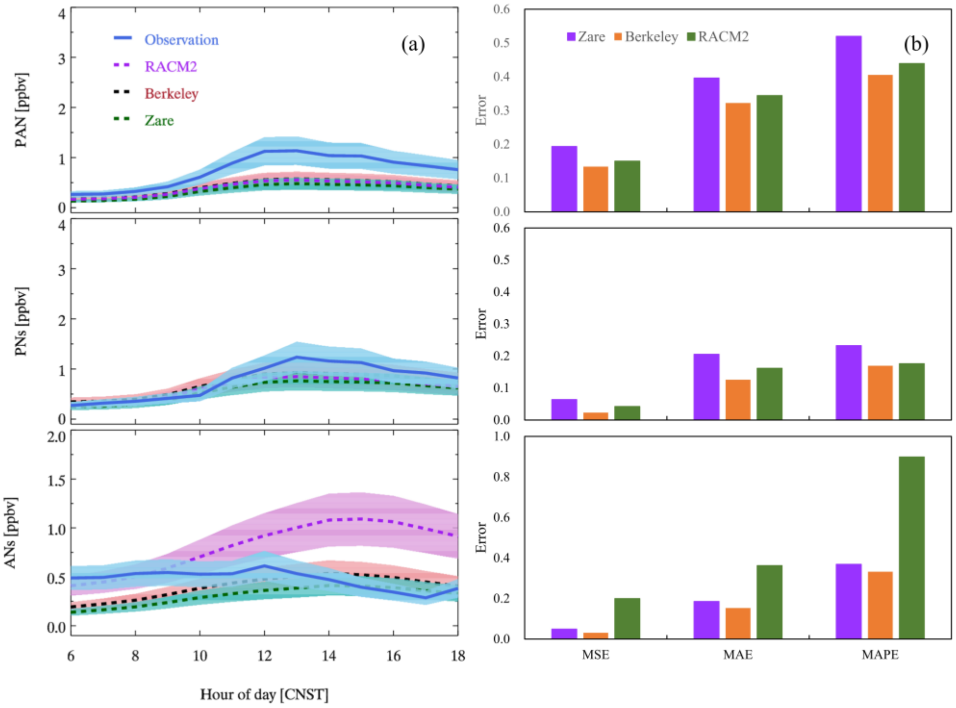

Figure 4. Mean diurnal profiles of observed and simulated ANs and PNs under different mechanism constraints during the Shanghai campaign (a), and the error of the different cases (b), including mean square error (MSE), mean absolute error (MAE) and mean absolute percentage error (MAPE).

3.3 Impact of PNs chemistry on local ozone production

Organic nitrates and O_3 have common precursors, and therefore the atmospheric behavior of organic nitrates has an important influence on the local O_3 distribution. The production of PNs consumes NO_2 and RO_x, thereby directly impacting O_3 production. The relationship between the distribution of PNs and O_3 is examined throughout the campaign. The observed PAN, PNs and O_3 between 9:00 a.m. and 2:00 p.m. are selected for the analysis to mitigate interference from sources that are not produced during daytime. The correlation of PAN or PNs with O_3 are shown in Fig. S2. Both PAN and PNs demonstrate a strong correlation with O_3 with the ratio of PAN or PNs to O_3 being 0.041 or 0.058. High ratios of PNs and O_3 usually indicate severe pollution episodes (Shepson et al., 1992; Sun et al., 2020; Zhang et al., 2023; Zhang et al., 2014). The minimum ratio of PNs to O_3 (0.024) was found during the clean periods, which can be regarded as the threshold for local photochemical pollution. NO_x is the key pollutant for production of O_3 and PNs, in order to study the relationship between the ratio of PAN or PNs to O_3 and NO_x. The daytime ratios of PAN to O_3 derived from historical field observations are summarized with corresponding NO_x concentrations in Fig. 5. The ratio derived from this study was distributed in the medium level of historical observations. The linear correlation of NO_x and the ratio of PAN to O_3 ratio suggests that the NO_x concentration controls the relative production of PNs and O_3.

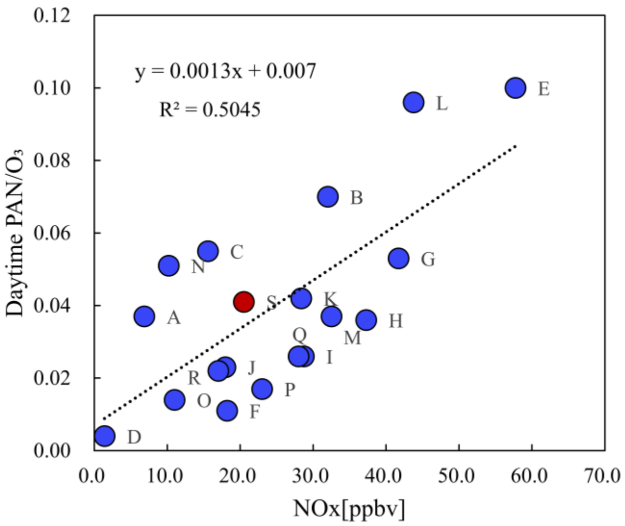

Figure 5. The relationship between historical daytime ratio of PAN to O_3 and NO_x concentrations. The red dot is the Shanghai campaign, and the blue dots are the historical campaigns. A: Grosjean et al., 2002 (Grosjean et al., 2002); B: Lee et al., 2008 (Lee et al., 2008), C: Zhang et al., 2014 (Zhang et al., 2014), D-E: Zhang et al., 2009 (Zhang et al., 2009), F-G: Zeng et al., 2019 (Zeng et al., 2019), H-K: Zhang et al., 2019 (Zhang et al., 2019), L-M: Sun et al., 2020 (Sun et al., 2020); N: Li et al., 2023 (Li et al., 2023), O-R: Xu et al., 2024 (Xu et al., 2024), S: this study.

Sensitivity tests were conducted based on the box model to quantify the impact of PNs photochemistry on O_3 budgets. The differences of each pathway rate are calculated at the peak of O_3 production rate (Fig. 6). In the absence of PNs chemistry, two primary source pathways -namely, the reaction between RO_2 and NO, and the reaction between HO_2 and NO-exhibit large enhancements of 0.52 and 0.36 ppbv/h, respectively. In comparison, O_3 sinks increase slightly in the absence of PNs photochemistry, with the reaction between OH and O_3 showing the most significant enhancement of 0.11 ppbv/h. Therefore, during the Shanghai campaign, PNs photochemistry suppressed daytime ozone production mainly by reducing the reaction between HO_2 or RO_2 and NO.

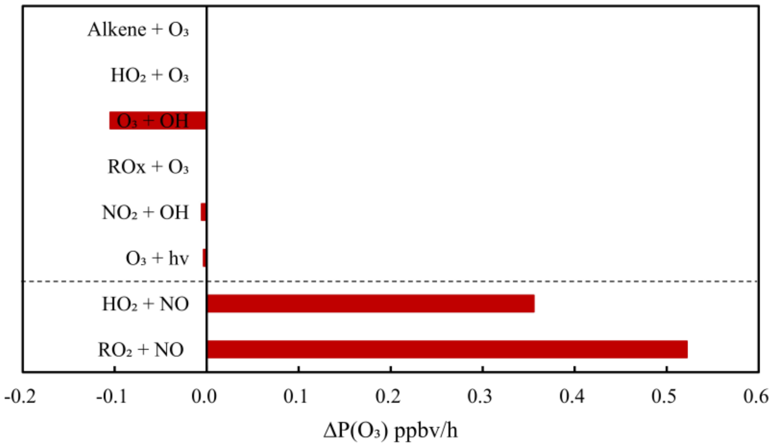

Figure 6. The simulated difference of ozone produce rate ($\Delta P(O_3)$) at 11am between the constraint of the PNs photochemistry and without the PNs photochemistry.

The PNs maintain a notable concentration until 6:00 p.m., suggesting a persistent impact on local ozone production. As shown in Fig. 7a, the PNs photochemistry began to inhibit ozone production as early as 6 a.m. and increased up to 0.8 ppbv/h (16%) at 10 a.m. The integrated inhibition of PNs photochemistry on O_3 production was 4.5 ppbv in the Shanghai campaign (Fig. 7b), which was less pronounced than the Xinjin campaign (20 ppbv). The reduced inhibition can be attributed to the lower PNs production rate (P(PNs)) observed in the Shanghai campaign (Fig. S3), where the maximum daytime P(PNs) was 0.89 ppbv/h, much lower than that in Xinjin campaign (3.09 ppbv/h). In addition, the two campaigns had similar concentrations of VOCs, but daytime average of NO_x in Shanghai site is 22.0 ppbv, which is much higher than that of Xinjin site (10.2 ppbv). The PNs formation would be reduced under high NO_x condition due to the rapid termination reaction via OH and NO_2, and thus limited the suppression effect of PNs formation which is the case in Shanghai campaign. Like in Xinjin campaign, PAN chemistry suppressed O_3 formation at a rate of 2.84 ppbv/h at a suburban site in Hong Kong (Zeng et al., 2019). However, it was reported that PAN tended to suppress O_3 production under low-NO_x and low-RO_x conditions but enhanced O_3 production with sufficient NO_x at a rural coastal site in Qingdao, which is consistent with the comparison of Xinjin and Shanghai campaigns (Liu et al., 2021). The impacts of PNs photochemistry on O_3 vary across different days. As shown in Fig. S4, the integrated $P(O_3)$ change reaches 6.9 ppbv due to PNs photochemistry during ozone pollution period. For the background and clean periods, the changes are close to each other with a value of 3.8 and 4.2 ppbv, respectively. Therefore, the PNs photochemistry contributes to more $P(O_3)$ inhibition during the ozone pollution period, which should be considered in ozone pollution prevention.

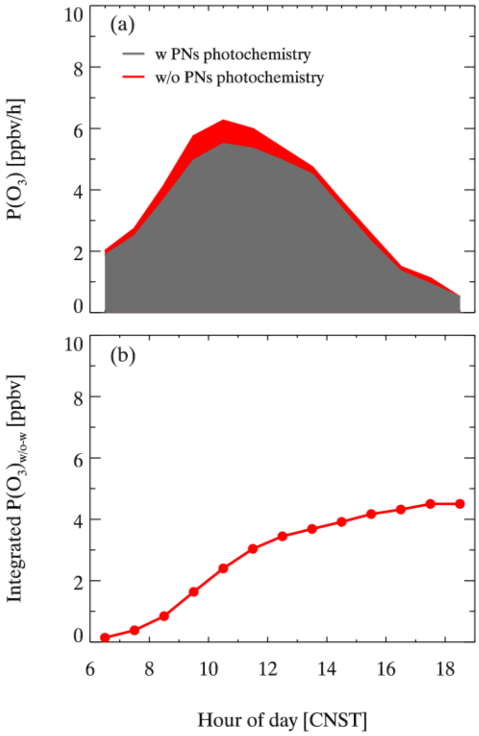

Figure 7. The impact of PNs photochemistry on $P(O_3)$ during the Shanghai campaign (a) daily changes of $P(O_3)$ under the constraint of PNs photochemistry, (b) integrated $P(O_3)$ change constrained by PNs photochemistry.

3.4 Impact of ANs chemistry on local ozone production

To elucidate the impact of the α on O_3 production, the EKMA was utilized to investigate the combined response of NO_x and VOCs to O_3 production at different α. The O_3 production was calculated by a simplified approach in method 2.2 and the α values were derived from weighted average of α based on the measured VOCs, the corresponding OH reaction rate constant and the α (Table S1) in Shanghai and Xinjin campaign, respectively. The model is initiated by the daytime averages of the environmental parameters. A comparative analysis is conducted between the Xinjin campaign and the Shanghai campaign where effective α is determined to be 0.031 and 0.053, respectively. As illustrated in Fig. 8a&b, $P(O_3)$ exhibits a similar trend with the variations of NO_x and VOCs under different α, while the value of $P(O_3)$ reduces with larger α at the same levels of precursors. For example, when VOCs is at 8 ppbv and NO_x reaches 9 ppbv, the $P(O_3)$ is 30.4 ppbv/h with α of 0.031, whereas it decreases to 24.6 ppbv/h when α is 0.053. In addition, the larger of α in the Shanghai campaign increases the threshold of NO_x concentration for the transition of O_3 production regime. When the concentration of VOCs is fixed, a higher effective α results in a lower NO_x concentration corresponding to the peak of $P(O_3)$. Consequently, an increase in α suppresses the peak of $P(O_3)$ and simultaneously affects its sensitivity to NO_x and VOCs concentrations.

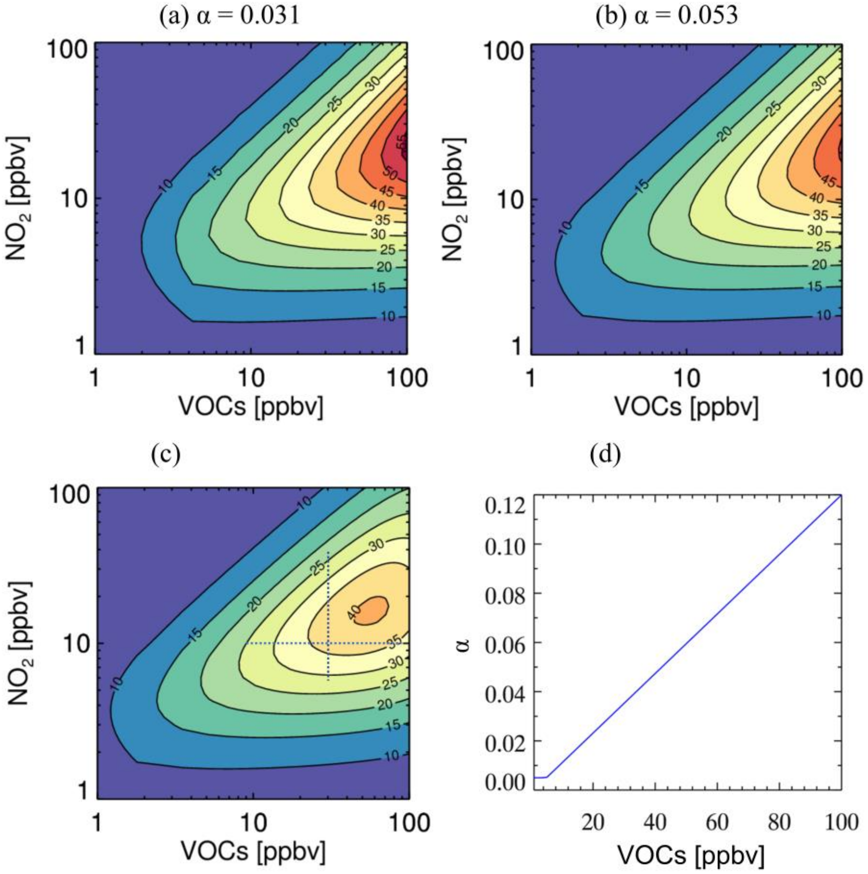

Figure 8. Ozone production ($P(O_3)$, ppb h-1) derived from a simplified analytic model is plotted as a function of NO_x and VOCs under three different organic nitrate scenarios with branching ratios of (a) 0.031 for the Xinjin campaign, (b) 0.053 for the Shanghai campaign, and (c)VOC-dependent branching ratios for Shanghai campaign, where the

branching ratio decreases linearly from 12 to 0.5% with VOCs from 100 to 5 ppbv as shown in (d).

In the real atmosphere, the effective α of ANs tends to exhibit a decline with the reduction of VOCs concentration. Historical studies show the general range from 0.03 to 0.04 in rural sites and from 0.04 to 0.10 in urban environments, depending on the composition of VOCs and the α for BVOCs (Farmer et al., 2011; Perring et al., 2010; Perring et al., 2013; Perring et al., 2009; Rosen et al., 2004b). For simplicity, we use a linear relationship between α and VOC concentration in the sensitivity analysis, as shown in Fig. 8d. An α value of 0.005 was selected for clean condition with VOC concentration less than 5 ppbv, while 0.12 was selected for polluted condition with VOC concentration larger than 100 ppbv. The lower limit of 0.005 is the average of the α for methane and ethylene. The upper limit of 0.12 is set as the reported value of the α for isoprene and the α for aromatic hydrocarbons are generally distributed around 0.1 (Perring et al., 2013). The assumption of this linear relationship between α and VOC concentration has also been applied in a previous study (Farmer et al., 2011). With a varying α, as shown in Fig. 8d, P(O_3) does not follow a consistent downward trend as VOCs decrease in VOC-limited regime or transition regime. Instead, with the decrease of VOCs, the P(O_3) is likely to increase at first at a relatively high VOCs distribution, and then decrease similar to the fixed α scenario. Take the cases of the horizontal dashed line as an example, at a fixed NO_x, the P(O_3) increases as the VOCs decrease within the range of about 60 to 100 ppbv, whereas P(O_3) subsequently decrease as VOCs fell below 60 ppbv. Therefore, with the reduction in VOCs emission, an increase in α directly correlates with a reduction in the P(O_3) peak. As a result, a positive correlation between α and VOCs concentrations in real atmosphere might alter the NO_x-VOCs-O_3 relationship and diminish the effects of VOCs reduction on ozone control.

Scenarios with different VOCs reactivity and α are selected for sensitivity tests to further investigate the impact of ANs chemistry on the O_3 pollution control strategy in Shanghai. As illustrated in Fig. 9a, variations of P(O_3) among three scenarios exhibit an initial increase followed by a subsequent decrease with rising NO_x. For the typical VOC reactivity and α obtained from the Shanghai campaign, the turning point from NO_x benefit to NO_x limitation for P(O_3) occurs at NO_x concentration of 1.38 ppbv, when P(O_3) reaches a peak of 33.0 ppbv/h. When VOCs are reduced by 20% without accounting for the reductions in α, the turning point for NO_x decreases to 1.26 ppbv with the P(O_3) peak decreasing to 30.1 ppbv/h. When the reduction of α is considered alongside the decrease in VOCs (α decreases to 0.0265), the peak of P(O_3) remains the same as the initial case. Consequently, neglecting the α changes is likely to overestimate the effectiveness of emission control. Our observations indicated that NO_x in Shanghai was notably high, which accords with the conditions to the right of the turning point in Fig. 9a. In this case, the major chain-termination reaction of the HO_x cycle is the reaction between OH and NO_2 to produce HNO_3, while the share of the reaction that produces ANs through the reaction between RO_2 and NO becomes relatively minor. As illustrated in Fig. 9a, when NO_x changes from 22.0 to 1.0 ppbv, the impact of α change will be larger, as the P(O_3) difference between the two cases ranges from 0.1 to 2.6 ppbv/h. Therefore, the variation of α has a limited impact on O_3 production at high NO_x, whereas it offsets the impact of VOCs reduction as NO_x decrease to around 1.5 ppbv which represents a low-NO_x emission condition. In addition, the sensitivity analyses in a reduced VOC condition show that neglecting the α change still overestimates the impact of VOCs reduction on P(O_3) by around 4 times with NO_x of 1 ppbv (Fig. 9b), which is also more significant than the case in Shanghai campaign. Therefore, the variation in α has a temporarily limited impact on O_3 production, whereas it should be seriously considered as NO_x levels continue to decrease.

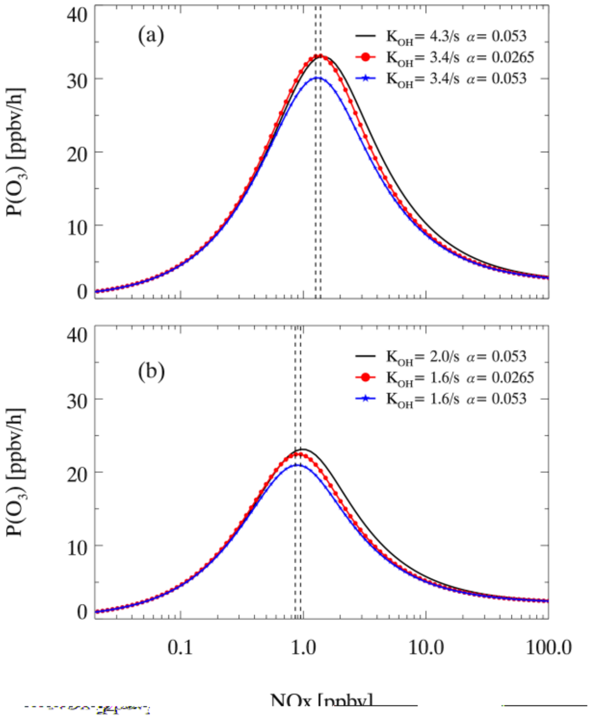

Figure 9. The ozone production rate (P(O_3)) varies as a function of NO_x under different VOC-NO_x regimes during Shanghai campaign: (a) under mean measured parameters during the whole campaign (solid line, VOC reactivity (K_{OH}) of 4.3/s, ANs branching ratio (α) of 0.053); a 20% reduction in K_{OH} with a 50% reduction in α (red dot line, 3.4/s, 0.0265); a 20% reduction in K_{OH} with no change in α (blue dot line, 3.4/s, 0.053). (b) under observed parameters during the clean days (solid line, K_{OH} of 2.0/s, α of 0.053); a 20% reduction in K_{OH} with a 50% reduction in α (red dot line, 1.6/s, 0.0265); a 20% reduction in K_{OH} with no change in α (blue dot line, 1.6/s, 0.053). Dash lines show the turning point in different cases.

To further investigate the effect of ANs formation on O_3 production during different days, sensitivity tests on VOCs reactivity and α are conducted based on typical conditions during different periods. The α values are derived as 0.055, 0.054 and 0.052, for the high ozone, clean and background periods, respectively. As shown in Fig. S4, the P(O_3) exhibits a similar trend with the increase of NO_x across different periods. The P(O_3) peak during the background period (30.3 ppbv/h) is slightly lower than that during both the high ozone days and the clean days (32.5 and 32.4 ppbv/h). Therefore, the ANs chemistry has similar effects on O_3 production within different periods during the Shanghai campaign. Further comparisons of ozone production under varying precursor levels were conducted using historical observations collected in August 1994 at Mecklenburg-Vorpommern Mankmoos (MK), Germany (Ehhalt, 1999), and during the spring of 2006 in Mexico City (MX) (Farmer et al., 2011; Perring et al., 2010). The MK site serves as a typical clean background location with a very low effective α of 0.005, corresponding to τVOC of 0.4 s^{-1}, where methane is the predominant pollutant. Conversely, the MX site is characterized as an urban environment with an effective α of 0.036, where a total of 58 VOCs was measured, corresponding to τVOC of 3.1s^{-1}. The MK site shows a peak of P(O_3) is 2.2 ppbv/h at the NO_x of 0.63 ppbv. In contrast, the MX site demonstrates a peak P(O_3) of 7.2 ppbv/h at a NO_x of 1.9 ppbv. Given that the Xinjin and Shanghai sites exhibit higher VOCs reactivity than MX, the corresponding peak P(O_3) and the NO_x inflection point are significantly elevated. This increase is primarily attributed to the high P(HO_x), coupled with a low α, which substantially enhances P(O_3) under the intensified HO_x cycling. Consequently, the ozone production potentials of urban sites in China are overall higher than in other regions, while the influence of α appears to be weak.

4. Conclusions

This study reveals the abundances of PNs and ANs and quantifies their respective impacts on O3 pollution based on the field campaign in Shanghai. They both showed higher values but less pronounced diurnal variation during the O_3 pollution period than the clean period. The mechanism validation indicates that Berkeley mechanism generally outperforms in the simulation of organic nitrates. The ratio of PNs/O_3 serves as a significant indicator of photochemistry. In comparison to the previous Xinjin campaign, the inhibition effect of PNs chemistry on daytime O_3 production diminished, likely attributed to the lower production of PNs. For ANs, the model simulation demonstrated that the branching ratio (α) influences the NO_x-VOCs-O_3 sensitivity. The consideration of α value not only alters the P(O_3) peak in EKMA but also resulted in low effectiveness of precursor reductions, as the α would change with the reduction of VOCs. It is worth mentioning that the complex polluted regions are usually characterized by high NO_x and HO_x. In that case, the contribution of chain-termination reactions that produce ANs could be reduced, leading to limited impact of AN chemistry on O_3 formation. The effect of ANs chemistry on O_3 pollution control is therefore expected to enhance with further precursor reductions, and we suggest a pressing need for more measurements and analysis of organic nitrates to address the forthcoming challenges in air pollution mitigation.

Code/Data availability. The datasets used in this study are available from the corresponding author upon request (chenxr95@mail.sysu.edu.cn; k.lu@pku.edu.cn).

Author contributions. K.D.L. and X.R.C. designed the study. C.M.L. and X.R.C. analyzed the data and wrote the paper with input from K.D.L.

Competing interests. The authors declare that they have no conflicts of interest.

Acknowledgments. This work was supported by the National Natural Science Foundation of China (Grants No. 42407139); the National Natural Science Foundation of China (Grants No. 22406204); the special fund of State Environmental Protection Key Laboratory of Formation and Prevention of Urban Air Pollution Complex (SEPAir-2024080219); the Innovative Exploration Program of National Institute of Metrology, China (No. AKYCX2313).

References

Arey J, Aschmann SM, Kwok ESC, Atkinson R. Alkyl Nitrate, Hydroxyalkyl Nitrate, and Hydroxycarbonyl Formation from the NOx−Air Photooxidations of C5−C8 n-Alkanes. The Journal of Physical Chemistry A 2001; 105: 1020-1027.

Aruffo E, Di Carlo P, Dari-Salisburgo C, Biancofiore F, Giammaria F, Busilacchio M, et al. Aircraft observations of the lower troposphere above a megacity: Alkyl nitrate and ozone chemistry. Atmospheric Environment 2014; 94: 479-488.

Ashmore MR. Assessing the future global impacts of ozone on vegetation. Plant Cell and Environment 2005; 28: 949-964.

Browne EC, Cohen RC, Wooldridge PJ, Valin LC, Min K-E. Organic nitrate formation: Impacts on NOx lifetime and ozone. Abstracts of Papers of the American Chemical Society 2012; 244.

Browne EC, Min KE, Wooldridge PJ, Apel E, Blake DR, Brune WH, et al. Observations of total RONO2 over the boreal forest: NOx sinks and HNO3 sources. Atmospheric Chemistry and Physics 2013; 13: 4543-4562.

Chen J, Wu H, Liu AW, Hu SM, Zhang J. Field Measurement of NO2 and RNO2 by Two-Channel Thermal Dissociation Cavity Ring Down Spectrometer. Chinese Journal of Chemical Physics 2017; 30: 493-498.

Darer AI, Cole-Filipiak NC, O'Connor AE, Elrod MJ. Formation and Stability of Atmospherically Relevant Isoprene-Derived Organosulfates and Organonitrates. Environmental Science & Technology 2011; 45: 1895-1902.

Day DA, Dillon MB, Wooldridge PJ, Thornton JA, Rosen RS, Wood EC, et al. On alkyl nitrates, O-3, and the "missing NOy". Journal of Geophysical Research-Atmospheres 2003; 108.

Ehhalt DH. Photooxidation of trace gases in the troposphere. Physical Chemistry Chemical Physics 1999; 1: 5401-5408.

Farmer DK, Perring AE, Wooldridge PJ, Blake DR, Baker A, Meinardi S, et al. Impact of organic nitrates on urban ozone production. Atmospheric Chemistry and Physics 2011; 11: 4085-4094.

Fisher JA, Jacob DJ, Travis KR, Kim PS, Marais EA, Miller CC, et al. Organic nitrate chemistry and its implications for nitrogen budgets in an isoprene- and monoterpene-rich atmosphere: constraints from aircraft (SEAC(4)RS) and ground-based (SOAS) observations in the Southeast US. Atmospheric Chemistry and Physics 2016; 16: 5969-5991.

Flocke F, Volz-Thomas A, Buers HJ, Patz W, Garthe HJ, Kley D. Long-term measurements of alkyl nitrates in southern Germany 1. General behavior and seasonal and diurnal variation. Journal of Geophysical Research-Atmospheres 1998; 103: 5729-5746.

Gao W, Tie X, Xu J, Huang R, Mao X, Zhou G, et al. Long-term trend of O-3 in a mega City (Shanghai), China: Characteristics, causes, and interactions with precursors. Science of the Total Environment 2017; 603: 425-433.

Grosjean E, Grosjean D, Woodhouse LF, Yang YJ. Peroxyacetyl nitrate and peroxypropionyl nitrate in Porto Alegre, Brazil. Atmospheric Environment 2002; 36: 2405-2419.

Ito A, Sillman S, Penner JE. Global chemical transport model study of ozone response to changes in chemical kinetics and biogenic volatile organic compounds emissions due to increasing temperatures: Sensitivities to isoprene nitrate chemistry and grid resolution. Journal of Geophysical Research-Atmospheres 2009; 114.

Lee G, Jang Y, Lee H, Han J-S, Kim K-R, Lee M. Characteristic behavior of peroxyacetyl nitrate (PAN) in Seoul megacity, Korea. Chemosphere 2008; 73: 619-628.

Li C, Wang H, Chen X, Zhai T, Chen S, Li X, et al. Thermal dissociation cavity-enhanced absorption spectrometer for measuring NO2, RO2NO2, and RONO2 in the atmosphere. Atmospheric Measurement Techniques 2021; 14: 4033-4051.

Li C, Wang H, Chen X, Zhai T, Ma X, Yang X, et al. Observation and modeling of organic nitrates on a suburban site in southwest China. Science of the Total Environment 2023; 859.

Liebmann J, Karu E, Sobanski N, Schuladen J, Ehn M, Schallhart S, et al. Direct measurement of NO3 radical reactivity in a boreal forest. Atmospheric Chemistry and Physics 2018; 18: 3799-3815.

Liebmann J, Sobanski N, Schuladen J, Karu E, Hellen H, Hakola H, et al. Alkyl nitrates in the boreal forest: formation via the NO3-, OH- and O-3-induced oxidation of biogenic volatile organic compounds and ambient lifetimes. Atmospheric Chemistry and Physics 2019; 19: 10391-10403.

Ling ZH, Guo H, Simpson IJ, Saunders SM, Lam SHM, Lyu XP, et al. New insight into the spatiotemporal variability and source apportionments of C-1-C-4 alkyl nitrates in Hong Kong. Atmospheric Chemistry and Physics 2016; 16: 8141-8156.

Liu Y, Shen H, Mu J, Li H, Chen T, Yang J, et al. Formation of peroxyacetyl nitrate (PAN) and its impact on ozone production in the coastal atmosphere of Qingdao, North China. Science of the Total Environment 2021; 778.

Lu KD, Hofzumahaus A, Holland F, Bohn B, Brauers T, Fuchs H, et al. Missing OH source in a suburban environment near Beijing: observed and modelled OH and HO<sub>2</sub> concentrations in summer 2006. Atmospheric Chemistry and Physics 2013; 13: 1057-1080.

Monks PS, Archibald AT, Colette A, Cooper O, Coyle M, Derwent R, et al. Tropospheric ozone and its precursors from the urban to the global scale from air quality to short-lived climate forcer. Atmos. Chem. Phys. 2015; 15: 8889-8973.

Ng NL, Brown SS, Archibald AT, Atlas E, Cohen RC, Crowley JN, et al. Nitrate radicals and biogenic volatile organic compounds: oxidation, mechanisms, and organic aerosol. Atmospheric Chemistry and Physics 2017; 17: 2103-2162.

Perring AE, Bertram TH, Farmer DK, Wooldridge PJ, Dibb J, Blake NJ, et al. The production and persistence of Sigma RONO2 in the Mexico City plume. Atmospheric Chemistry and Physics 2010; 10: 7215-7229.

Perring AE, Pusede SE, Cohen RC. An Observational Perspective on the Atmospheric Impacts of Alkyl and Multifunctional Nitrates on Ozone and Secondary Organic Aerosol. Chemical Reviews 2013; 113: 5848-5870.

Perring AE, Wisthaler A, Graus M, Wooldridge PJ, Lockwood AL, Mielke LH, et al. A product study of the isoprene+NO3 reaction. Atmospheric Chemistry and Physics 2009; 9: 4945-4956.

Present PSR, Zare A, Cohen RC. The changing role of organic nitrates in the removal and transport of NOx. Atmospheric Chemistry and Physics 2020; 20: 267-279.

Reisen F, Aschmann SM, Atkinson R, Arey J. 1,4-hydroxycarbonyl products of the OH radical initiated reactions of C-5-C-8 n-alkanes in the presence of N0. Environmental Science & Technology 2005; 39: 4447-4453.

Roberts JM, Bertman SB. The thermal-decomposition of peroxyacetic nitric anhydride (pan) and peroxymethacrylic nitric anhydride (MPAN). International Journal of Chemical Kinetics 1992; 24: 297-307.

Romer PS, Duffey KC, Wooldridge PJ, Allen HM, Ayres BR, Brown SS, et al. The lifetime of nitrogen oxides in an isoprene-dominated forest. Atmospheric Chemistry and Physics 2016; 16: 7623-7637.

Romer PS, Duffey KC, Wooldridge PJ, Edgerton E, Baumann K, Feiner PA, et al. Effects of temperature-dependent NOx emissions on continental ozone production. Atmospheric Chemistry and Physics 2018; 18: 2601-2614.

Rosen RS, Wood EC, Wooldridge PJ, Thornton JA, Day DA, Kuster W, et al. Observations of total alkyl nitrates during Texas Air Quality Study 2000: Implications for O-3 and alkyl nitrate photochemistry. Journal of Geophysical Research-Atmospheres 2004a; 109: 15.

Rosen RS, Wood EC, Wooldridge PJ, Thornton JA, Day DA, Kuster W, et al. Observations of total alkyl nitrates during Texas Air Quality Study 2000: Implications for O-3 and alkyl nitrate photochemistry. Journal of Geophysical Research-Atmospheres 2004b; 109.

Sadanaga Y, Takaji R, Ishiyama A, Nakajima K, Matsuki A, Bandow H. Thermal dissociation cavity attenuated phase shift spectroscopy for continuous measurement of total peroxy and organic nitrates in the clean atmosphere. Review of Scientific Instruments 2016; 87.

Schwantes RH, Emmons LK, Orlando JJ, Barth MC, Tyndall GS, Hall SR, et al. Comprehensive isoprene and terpene gas-phase chemistry improves simulated surface ozone in the southeastern US. Atmospheric Chemistry and Physics 2020; 20: 3739-3776.

Shepson PB, Hastie DR, So KW, Schiff HI. Relationships between PAN, PPN and O3 at urban and rural sites in Ontario. Atmospheric Environment Part a-General Topics 1992; 26: 1259-1270.

Song J, Zhang Y, Huang Y, Ho KF, Yuan Z, Ling Z, et al. Seasonal variations of C-1-C-4 alkyl nitrates at a coastal site in Hong Kong: Influence of photochemical formation and oceanic emissions. Chemosphere 2018; 194: 275-284.

Sun J, Li Z, Xue L, Wang T, Wang X, Gao J, et al. Summertime C-1-C-5 alkyl nitrates over Beijing, northern China: Spatial distribution, regional transport, and formation mechanisms. Atmospheric Research 2018; 204: 102-109.

Sun M, Cui Jn, Zhao X, Zhang J. Impacts of precursors on peroxyacetyl nitrate (PAN) and relative formation of PAN to ozone in a southwestern megacity of China. Atmospheric Environment 2020; 231.

Tan Z, Fuchs H, Lu K, Hofzumahaus A, Bohn B, Broch S, et al. Radical chemistry at a rural site (Wangdu) in the North China Plain: observation and model calculations of OH, HO2 and RO2 radicals. Atmos. Chem. Phys. 2017a; 17: 663-690.

Tan Z, Fuchs H, Lu K, Hofzumahaus A, Bohn B, Broch S, et al. Radical chemistry at a rural site (Wangdu) in the North China Plain: observation and model calculations of OH, HO<sub>2</sub> and RO<sub>2</sub> radicals. Atmospheric Chemistry and Physics 2017b; 17: 663-690.

Tan Z, Lu K, Jiang M, Su R, Dong H, Zeng L, et al. Exploring ozone pollution in Chengdu, southwestern China: A case study from radical chemistry to O3-VOC-NOx sensitivity. Sci Total Environ 2018a; 636: 775-786.

Tan ZF, Rohrer F, Lu KD, Ma XF, Bohn B, Broch S, et al. Wintertime photochemistry in Beijing: observations of ROx radical concentrations in the North China Plain during the BEST-ONE campaign. Atmospheric Chemistry and Physics 2018b; 18: 12391-12411.

Teng AP, Crounse JD, Lee L, St Clair JM, Cohen RC, Wennberg PO. Hydroxy nitrate production in the OH-initiated oxidation of alkenes. Atmospheric Chemistry and Physics 2015; 15: 4297-4316.

Travis KR, Jacob DJ, Fisher JA, Kim PS, Marais EA, Zhu L, et al. Why do models overestimate surface ozone in the Southeast United States? Atmospheric Chemistry and Physics 2016; 16: 13561-13577.

Wang M, Shao M, Chen W, Lu S, Wang C, Huang D, et al. Measurements of C1-C4 alkyl nitrates and their relationships with carbonyl compounds and O-3 in Chinese cities. Atmospheric Environment 2013; 81: 389-398.

Wang W, Parrish DD, Wang S, Bao F, Ni R, Li X, et al. Long-term trend of ozone pollution in China during 2014–2020: distinct seasonal and spatial characteristics and ozone sensitivity. Atmospheric Chemistry and Physics 2022; 22: 8935-8949.

Xu T, Nie W, Xu Z, Yan C, Liu Y, Zha Q, et al. Investigation on the budget of peroxyacetyl nitrate (PAN) in the Yangtze River Delta: Unravelling local photochemistry and regional impact. Science of the Total Environment 2024; 917.

Xue K, Zhang X. The rationale behind updates to ambient ozone guidelines and standards. Frontiers in Public Health 2023; 11.

Yeh GK, Ziemann PJ. Alkyl Nitrate Formation from the Reactions of C₈-C₁₄ <i>n</i>-Alkanes with OH Radicals in the Presence of NO<i>_x</i>: Measured Yields with Essential Corrections for Gas-Wall Partitioning. Journal of Physical Chemistry A 2014a; 118: 8147-8157.

Yeh GK, Ziemann PJ. Identification and Yields of 1,4-Hydroxynitrates Formed from the Reactions of C₈-C₁₆ <i>n</i>-Alkanes with OH Radicals in the Presence of NO<i>_x</i>. Journal of Physical Chemistry A 2014b; 118: 8797-8806.

Young PJ, Naik V, Fiore AM, Gaudel A, Guo J, Lin MY, et al. Tropospheric Ozone Assessment Report: Assessment of global-scale model performance for global and regional ozone distributions, variability, and trends. Elementa-Science of the Anthropocene 2018; 6.

Zare A, Romer PS, Tran N, Keutsch FN, Skog K, Cohen RC. A comprehensive organic nitrate chemistry: insights into the lifetime of atmospheric organic nitrates. Atmospheric Chemistry and Physics 2018; 18: 15419-15436.

Zeng L, Fan G-J, Lyu X, Guo H, Wang J-L, Yao D. Atmospheric fate of peroxyacetyl nitrate in suburban Hong Kong and its impact on local ozone pollution. Environmental Pollution 2019; 252: 1910-1919.

Zhang B, Zhao X, Zhang J. Characteristics of peroxyacetyl nitrate pollution during a 2015 winter haze episode in Beijing. Environmental Pollution 2019; 244: 379-387.

Zhang G, Xia L, Zang K, Xu W, Zhang F, Liang L, et al. The abundance and inter-relationship of atmospheric peroxyacetyl nitrate (PAN), peroxypropionyl nitrate (PPN), O-3, and NOy during the wintertime in Beijing, China. Science of the Total Environment 2020; 718.

Zhang H, Tong S, Zhang W, Xu Y, Zhai M, Guo Y, et al. A comprehensive observation on the pollution characteristics of peroxyacetyl nitrate (PAN) in Beijing, China. Science of the Total Environment 2023; 905.

Zhang H, Xu X, Lin W, Wang Y. Wintertime peroxyacetyl nitrate (PAN) in the megacity Beijing: Role of photochemical and meteorological processes. Journal of Environmental Sciences 2014; 26: 83-96.

Zhang JM, Wang T, Ding AJ, Zhou XH, Xue LK, Poon CN, et al. Continuous measurement of peroxyacetyl nitrate (PAN) in suburban and remote areas of western China. Atmospheric Environment 2009; 43: 228-237.

Zhu W, Zhou M, Cheng Z, Yan N, Huang C, Qiao L, et al. Seasonal variation of aerosol compositions in Shanghai, China: Insights from particle aerosol mass spectrometer observations. Science of The Total Environment 2021; 771: 144948.